8. C. B. Murray, C. R. Kagan, M. G. Bawendi, *Science* **270**, 1335 (1995).
9. A. Berman, L. Addadi, S. Weiner, *Nature* **331**, 546 (1988).
10. A. Berman *et al.*, *Science* **250**, 664 (1990).
11. G. Falini, S. Albeck, S. Weiner, L. Addadi, *ibid.* **271**, 67 (1996).
12. B. Lawn, *Fracture of Brittle Solids* (Cambridge Univ. Press, Cambridge, 1993), chap. 6.
13. C. C. Harrison, *Phytochemistry* **41**, 37 (1996).
14. J. Aizenberg, G. Lambert, L. Addadi, S. Weiner, *Adv. Mater.* **8**, 222 (1996).
15. G. L. Becker, C. H. Chen, J. W. Greenwalt, A. L. Lehninger, *J. Cell Biol.* **61**, 316 (1974).
16. A. S. Posner, F. Betts, N. C. Blumenthal, *Metab. Bone Dis. Relat. Res.* **1**, 179 (1978).
17. S. Schultze-Lam, G. Harauz, T. J. Beveridge, *J. Bacteriol.* **174**, 7971 (1992).
18. S. Schultze-Lam, D. Fortin, B. S. Davis, T. J. Beveridge, *Chem. Geol.* **132**, 171 (1996).
19. S. I. Stupp and G. W. Ciegler, *J. Biomed. Mater. Res.* **26**, 169 (1992).
20. S. I. Stupp, G. C. Mejicano, J. A. Hanson, *ibid.* **27**, 289 (1993).
21. S. I. Stupp, J. A. Hanson, J. A. Eurell, G. W. Ciegler, A. Johnson, *ibid.*, p. 301.
22. S. I. Stupp, L. S. Li, M. Keser, in preparation.
23. N. A. Peppas and R. Langer, *Science* **263**, 1715 (1994).
24. J. A. Hubbell, *Bio/Technology* **13**, 565 (1995).
25. S. I. Stupp, A. Galan, M. Surhbur, S. Son, J. J. Hwang, in preparation.
26. J. J. Hwang, J. Hancock, K. Jaeger, S. I. Stupp, in preparation.
27. W. D. Kingery, H. K. Bowen, D. R. Uhlmann, *Introduction to Ceramics* (Wiley, New York, 1976).
28. J. S. Beck *et al.*, *J. Am. Chem. Soc.* **114**, 10834 (1992).
29. A. Monnier *et al.*, *Science* **261**, 1299 (1993).
30. Q. Huo *et al.*, *Nature* **368**, 317 (1994).
31. A. Firouzi *et al.*, *Science* **267**, 1138 (1995).
32. H. Yang, A. Kuperman, N. Coombs, S. Mamiche-Afara, G. A. Ozin, *Nature* **379**, 703 (1996).
33. P. T. Tanev, M. Chibwe, T. J. Pinnavaia, *ibid.* **368**, 321 (1994).
34. Z.-R. Tian *et al.*, *Science* **276**, 926 (1997).
35. Many papers on mesoporous materials have been published recently [for reviews, see J. S. Beck and J. C. Vartuli, *Curr. Opin. Solid State Mater. Sci.* **1**, 76 (1996); J. Liu *et al.*, *Adv. Colloid Interface Sci.* **69**, 131 (1996)].
36. H. Yang, N. Coombs, I. Sokolov, G. A. Ozin, *Nature* **381**, 589 (1996).
37. H. Yang, N. Coombs, G. A. Ozin, *ibid.* **386**, 692 (1997).
38. A typical surfactant used is cetyltrimethylammonium chloride or other quaternary ammonium surfactants of structure $C_nH_{2n+1}(CH_3)_3NX$, where X is Cl or Br and $n = 8$ to 22.
39. X. Feng *et al.*, *Science* **276**, 923 (1997).
40. G. M. Whitesides, *Sci. Am.* **273**, 146 (September 1995).
41. B. C. Bunker *et al.*, *Science* **264**, 48 (1994).
42. P. Rieke *et al.*, *Langmuir* **10**, 619 (1994).
43. P. B. Messersmith and S. I. Stupp, *Mater. Res. Soc. Symp. Proc.* **245**, 191 (1992)..
44. P. Osenar, P. B. Messersmith, S. I. Stupp, in preparation.
45. C. E. Becze and G. Xu, *J. Mater. Res.* **12**, 566 (1997).
46. N. Herron, J. C. Calabrese, W. E. Farneth, Y. Wang, *Science* **259**, 1426 (1993).
47. C. B. Murray, D. J. Norris, M. G. Bawendi, *J. Am. Chem. Soc.* **115**, 8706 (1993).
48. J. H. Fendler and F. C. Meldrum, *Adv. Mater.* **7**, 607 (1995).
49. T. Vossmeyer *et al.*, *Science* **267**, 1476 (1995).
50. X. Peng, T. E. Wilson, A. P. Alivisatos, P. G. Schultz, *Angew. Chem. Int. Ed. Engl.* **36**, 145 (1997).
51. E. M. Landau, *Mol. Cryst. Liq. Cryst.* **134**, 323 (1986).
52. Semiconductor growth can also be accomplished in phase-separated diblock copolymers [see C. C. Cummins, R. R. Schrock, R. E. Cohen, *Chem. Mater.* **4**, 27 (1992)], but in these systems, the organic matrix represents a significant volume fraction and cannot be removed without disrupting the microstructure of the semiconductor. It is also possible to prepare them in reverse micelles [see M. P. Pileni, *J. Phys. Chem.* **97**, 6961 (1993)].
53. V. Tohver, P. V. Braun, M. U. Pralle, S. I. Stupp, *Chem. Mater.* **9**, 1495 (1997).
54. Other inorganics for which this approach has worked include CdSe and ZnS (P. V. Braun, P. Osenar, V. Tohver, S. B. Kennedy, S. I. Stupp, in preparation).
55. D. Weiss *et al.*, *Phys. Rev. Lett.* **66**, 2790 (1991).
56. R. Fleischmann, T. Geisel, R. Ketzmerick, *ibid.*. **68**, 1367 (1992).
57. W. Kang, H. L. Stormer, L. N. Pfeiffer, K. W. Baldwin, K. W. West, *ibid.* **71**, 3850 (1993).
58. Generally, the particles obtained in these syntheses retain a small ($\leq$15% by volume) amount of organic material after work-up, and because the particles consist of a continuum of inorganic material, they are morphologically stable even after removal of most of the organic. Precipitation in the lamellar system generates a composite structure that is about 50 volume % organic of alternating sheets containing CdS and amphiphile. The strong affinity of the polar oligovinyl alcohol segments for the CdS results in a structure that is stable to repeated sonication in good solvents for the organic component, always retaining the lamellar structure.
59. D. B. Mitzi, C. A. Feild, W. T. A. Harrison, A. M. Guloy, *Nature* **369**, 467 (1994).
60. D. B. Mitzi, S. Wang, C. A. Feild, C. A. Chess, A. M. Guloy, *Science* **267**, 1473 (1995).
61. Y. Tian, C. Wu, N. Kotov, J. H. Fendler, *Adv. Mater.* **6**, 959 (1994).
62. J. H. Fendler, *Membrane-Mimetic Approach to Advanced Materials* (Springer-Verlag, Berlin, 1994).
63. S. I. Stupp *et al.*, *Science* **276**, 384 (1997).
64. P. Osenar, P. V. Braun, S. I. Stupp, *Adv. Mater.* **8**, 1022 (1996).
65. Supported by NIH—National Institute of Dental Research grant DE 05945, the Air Force Office of Scientific Research grant 90-0242, and the U.S. Department of Energy, Division of Materials Science grant DEFG02-96ER45439 through the University of Illinois at Urbana-Champaign, Frederick Seitz Materials Research Laboratory. We thank L. Addadi, C. C. Harrison, and S. Schultze-Lam for providing the electron micrographs in Fig. 1; M. G. Bawendi for providing one of the micrographs in Fig. 6; and M. Keser of the authors' laboratory for assistance with molecular graphics. A Beckman Institute graduate assistantship for P.V.B. is gratefully acknowledged.

Pathways to Macroscale Order in Nanostructured Block Copolymers

Zhong-Ren Chen, Julia A. Kornfield,* Steven D. Smith,
Jeffrey T. Grothaus, Michael M. Satkowski

Polymeric materials undergo dramatic changes in orientational order in response to dynamic processes, such as flow. Their rich cascade of dynamics presents opportunities to create and combine distinct alignments of polymeric nanostructures through processing. In situ rheo-optical measurements complemented by ex situ x-ray scattering reveal the physics of three different trajectories to macroscopic alignment of lamellar diblock copolymers during oscillatory shearing. At the highest frequencies, symmetry arguments explain the transient development of a bimodal texture en route to the alignment of layers parallel to the planes of shear. At lower frequencies, larger-scale relaxations introduce rearrangements out of the deformation plane that permit the formation of lamellae perpendicular to the shear plane. These explain the change in the character of the pathway to parallel alignment and the emergence of perpendicular alignment as the frequency decreases.

Self-assembly of block copolymers (*1*–*7*), surfactants (*8*–*11*), colloidal suspensions (*8*, *12*), and proteins (*13*) provides a versatile means to create nanostructures with potential applications in biomaterials, optics, and microelectronics. These materials form ordered structures on scales from a few to hundreds of nanometers. Monodisperse, charged colloidal suspensions can assemble three-dimensional lattices (*8*). Surfactant systems form a variety of morphologies and can be used as precursors to prepare nanostructured solid materials (*10*). Similarly, block copolymers (BCPs) assemble a fascinating array of nanostructures. BCPs have the desirable feature that their morphology can be systematically controlled by varying the number of blocks, their lengths, and their chemical compositions. For example, diblock copolymers can form cubic arrays of spheres, hexagonal arrays of cylinders, bicontinuous cubic phases, or lamellae, depending on the relative block lengths (*1*). Triblock copolymers composed of three distinct blocks (ABC) can assemble even more complex structures (*14*), such as helical strands surrounding cylinders embedded

---

Z.-R. Chen and J. A. Kornfield, California Institute of Technology, Chemical Engineering 210–41, Pasadena, CA 91125, USA.
S. D. Smith, J. T. Grothaus, M. M. Satkowski, Procter and Gamble, Miami Valley Laboratories, Cincinnati, OH 45239, USA.

*To whom correspondence should be addressed.

in a continuous matrix. Polymers also offer a level of control of dynamics that is desirable for scientific investigation and technological applications. Thus, block copolymers can clarify both the thermodynamics and dynamics of self-assembly phenomena that are analogous to those in a range of synthetic and biological systems, and can provide routes to the creation of novel materials.

Inducing Orientation in Self-Assembled Materials

The dynamics of self-assembled nanostructures assume special importance in the context of producing functional macroscopic materials, because self-assembly alone usually leads to polydomain structures with random orientations. To achieve desired directional properties, it is essential to control macroscale order. Active processing with applied fields can extend self-assembled order to macroscopic dimensions in BCPs (*1–4, 15–29*), colloidal suspensions (*12*), and surfactant systems (*9*). Flow has proven to be particularly efficient and versatile. In the case of BCPs, flow-induced alignment was first discovered by Keller in an extruded BCP (*2*). Since then, other flow methods, including oscillatory and steady shear, roll casting (*17*), and extensional flow (*18*), have been applied to many kinds of self-assembled systems. We focus on oscillatory shear in this article, because it permits systematic investigation of the coupled effects of the rate and amplitude of deformation in relation to the relaxation dynamics of the nanostructure.

Especially since the discovery of "flipping" (*16*), vigorous effort has been devoted to understanding flow-induced alignment in ordered BCPs (*5, 6, 16–31*). The term "flipping" was coined to describe a change in the alignment behavior of a lamellar structure under the influence of oscillatory shear: Depending on the shearing frequency and temperature, the final aligned state could be either parallel or perpendicular (Fig. 1) (*16*). Discovery of a means to induce two such different alignments opened up the possibility of producing radically different macroscopic materials from the same polymer, with relatively minor changes being made in processing conditions. The discovery also invited researchers to seek combinations of macromolecular structure and processing conditions that might allow the two alignments to be flipped back and forth, which would provide the basis for switchable optical, transport, and electronic properties.

To design functional materials that use the flipping phenomenon, the physical basis of the effects of molecular architecture and processing conditions (especially frequency, strain, and temperature) must be understood. Essential information on the dynamic responses that determine the distinct alignment regimes has been elusive, because conventional methods of characterizing the form and orientation distribution of an ordered structure are not amenable to providing information on the way it moves during flow. Transmission electron microscopy (TEM) involves the removal of samples from the flow device, followed by sectioning, staining, and imaging. Small-angle x-ray and neutron scattering (SAXS and SANS) measurements can be performed in situ during flow but do not provide adequate time resolution (published results are limited to times on the order of 100 s between scattering patterns) (*22, 29*). Although there is no substitute for the critical information these methods provide, they have been dramatically enhanced by the introduction of optical methods of characterizing the development of alignment in situ during flow that have ~10-ms time resolution (*23, 27, 28*).

The present study combines these two approaches. Rheo-optical methods of observing the alignment process in real time are used to guide the structural characterization of intermediate states along distinct paths to alignment. This strategy enables the clear association of microstructural changes with specific stages of each alignment trajectory. The results reveal the central physics of the processes leading to parallel and perpendicular orientations. On the basis of the observed processes, we propose a physical framework for understanding the transition between parallel and perpendicular alignment regimes as well as the qualitatively different routes to parallel orientation.

Theories of Alignment

Theoretical arguments to explain the alignment regimes have focused on the relative stability of distinct well-aligned states. The transverse alignment (Fig. 1) is the most unstable, because the equilibrium spacing is disturbed by shearing. Fluctuations on a layered structure can couple to shear if the lamellae are in the parallel orientation, making this alignment less stable than the perpendicular one (*6, 11*). However, the effect of fluctuations will be confined to frequencies (ω) that are fast enough that the fluctuations are not averaged out ($\omega > \omega_d$) and slow enough that distortion of the nanostructure is not overwhelmed by more local responses, such as conformational distortion of the polymer chains ($\omega < \omega_c$). Parallel alignment is predicted to be more stable than perpendicular alignment below a critical frequency controlled by the characteristic lifetime of fluctuations ($\omega < \omega_d$) (*11*). At frequencies higher than the conformational relaxation of the chains ($\omega > \omega_c$), the deformation couples to more local dynamics, and differences between the types of layers in the ordered structure can be probed. If there is considerable difference in the mechanical properties of the two types of layers, the modulus of the parallel state is lower than that of the perpendicular state; it has been argued that this explains the selection of parallel alignment at high frequencies ($\omega > \omega_c$) (*24*). These concepts can explain the three frequency regimes that have been observed (*1, 32*): Oscillatory strain amplitude γ_0 shearing can induce parallel alignment at $\omega < \omega_d$ (*33*), perpendicular alignment at $\omega_d < \omega < \omega_c$, and parallel alignment at $\omega_c < \omega$ (when the layers have dissimilar viscoelastic properties).

Theory regarding the relative stability of monodomains, although providing a valuable guide to experiment, has certain intrinsic limitations. The relative lack of theory and simulation (*34*) of the progressive development of alignment leaves us without predictions of what conditions are required to reach a monodomain state and how molecular and processing parameters affect the rate of the process.

Experimental Studies of Flow Alignment

To guide theoretical treatment of the dynamics of flow-induced orientation, we provide structural information on the changes

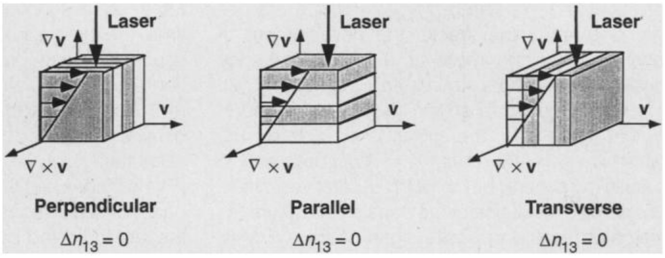

Fig. 1. Schematic diagram of the macroscale alignments that can be induced in lamellar block copolymers: perpendicular and parallel. The third principal projection is termed transverse. When probed by light propagating along the velocity gradient direction, the birefringence Δn_{13} of a lamellar PS-PI diblock is positive for perpendicular, zero for parallel, and negative for transverse orientations.

that occur along three distinct pathways to alignment (Fig. 2). The material was a nearly symmetrical styrene-isoprene diblock (weight-averaged molecular weight $M_w \approx$ 20 kg/mol; order-disorder transition (ODT) temperature T_{ODT} = 172°C) (*27*, *28*, *35*). The progress of alignment was monitored in situ by the birefringence observed in the (**v**, $\nabla\times$**v**)-plane (Fig. 1) with a rheo-optical instrument (*23*, *27*). The pathway to perpendicular alignment was characterized by the buildup of a large positive birefringence (top curve, Fig. 2). Perpendicular alignment was observed at sufficiently large strains over a wide range of temperatures (0.8 $T_{ODT} < T < T_{ODT}$) and frequencies (0.0001 $\omega_c < \omega < \omega_c$) in polystyrene-polyisoprene diblocks that were heated through the ODT to erase their flow and thermal history and then were cooled to the temperature at which shear-induced alignment was subsequently performed (*27*, *28*, *33*). The other two trajectories are representative of two qualitatively different routes to parallel alignment at high frequencies (in the polymeric regime, $\omega > \omega_c$): the first (middle curve, Fig. 2) is characteristic of a family of trajectories observed at sufficiently large strains in a narrow range of frequencies only modestly above ω_c ($\omega_c < \omega < 10\omega_c$), and the second (bottom curve, Fig. 2) is representative of the family of trajectories that is found at higher frequencies ($10\omega_c < \omega$) (*36*).

A representative path to perpendicular alignment was characterized by taking samples in the middle of the initial "fast" process, in the region where the character of the process changes (*28*), and in the middle of the subsequent "slow" process (points A, B, and C along the top curve in Fig. 2). During the earliest stages of the process (up to point A), the initial, nearly isotropic orientation of the lamellae (*35*) becomes enriched in the parallel and perpendicular projections and in all orientations in between, as indicated by the growth of intensity in the whole ring observed in the (∇**v**, $\nabla\times$**v**) plane (Fig. 3A), with a preferential enrichment of the perpendicular projection indicated by the peaks in the (∇**v**, $\nabla\times$**v**) and (**v**, $\nabla\times$**v**) planes. Continuing through the fast process to point B, there is greater selectivity in the enhancement of the perpendicular projection (increasing intensity in peaks along $\nabla\times$**v**, Fig. 3B) but not yet an elimination of the parallel and intermediate orientations [the ring of intensity in the (∇**v**, $\nabla\times$**v**) plane]. In contrast, the slow process from point B to C brings both further increases in the perpendicular projection and progressive elimination of the other orientations generated earlier (compare blue to green curves, Fig. 3, bottom). This trend continues from point C to the completion of alignment, based on SAXS patterns of the final aligned state (*28*).

The trajectory to parallel alignment at frequencies only modestly above the transition to the polymeric regime ($\omega_c < \omega < 10\omega_c$) began in a way similar to the initial stages of the perpendicular alignment trajectory. The primary change during the fast process (from the initial state to points A and B, middle curve, Fig. 2) was the conversion of poorly organized regions into well-defined lamellae [see TEM results in (*35*)]. This process was anisotropic and favored the creation of layers perpendicular to the plane of the gradient and neutral directions (Fig. 1), as indicated by the growth of the whole ring of intensity in the (∇**v**, $\nabla\times$**v**) plane (Fig. 4, A and B). In this frequency regime, though, the parallel alignment is enhanced most strongly (peaks along ∇**v**). Beyond this point (B, middle curve, Fig. 2), the character of the process changed: The birefringence no longer increased, and the effect of strain on the rate of the process became weaker than it was in the fast process (*27*, *28*). During the subsequent slow process, the domains grew in size (*35*), and the perpendicular component of the orientation distribution was reduced as the parallel component became more and more dominant (Fig. 4C). Samples removed after much longer times showed sharp x-ray peaks corresponding to a highly aligned par-

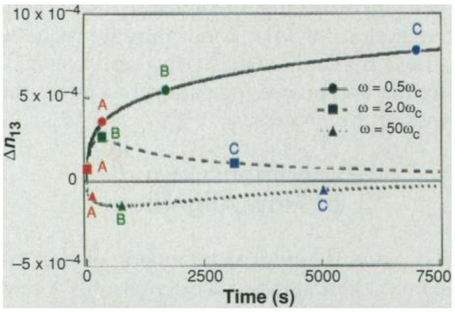

Fig. 2. Three trajectories of shear-induced alignment in a PS-PI diblock copolymer as revealed by real-time measurements of their birefringence Δn_{13} (all at T = 115°C; T/T_{ODT} = 0.87). The upper one (solid line) tracks the development of perpendicular alignment at a shear frequency $\omega < \omega_c$ (ω = 1 rad/s strain amplitude, γ_0 = 60%). The middle one (dashed line) ($\omega > \omega_c$:ω = 4 rad/s, γ_0 = 70%) and the lower one (dotted line) ($\omega \gg \omega_c$: ω = 100 rad/s, γ_0 = 30%) both lead to parallel alignment, but through qualitatively different paths of evolution of the transient structure, as indicated by the opposite signs of Δn_{13}. For all three trajectories, we took samples for ex situ characterization at three intermediate states marked A, B, and C.

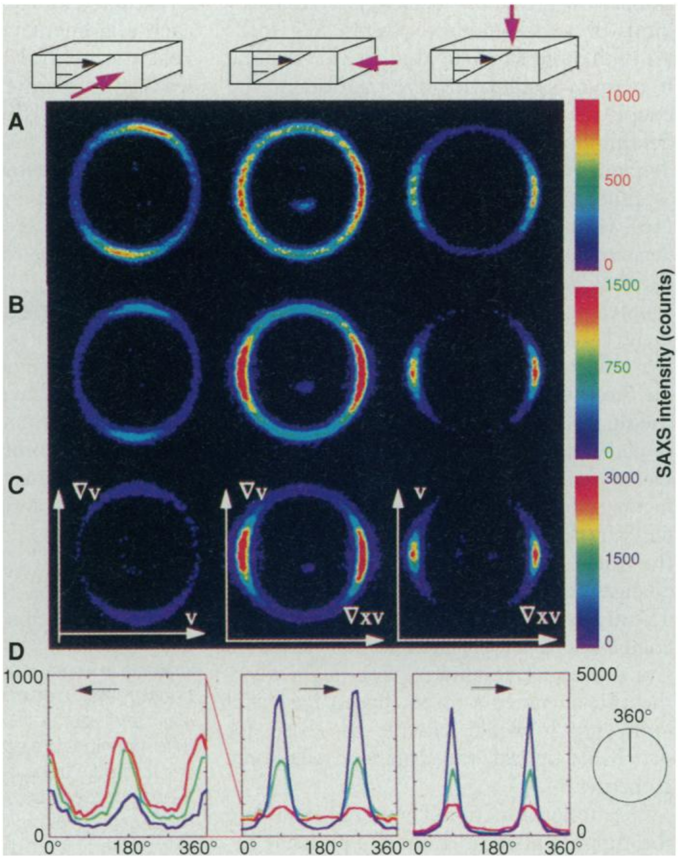

Fig. 3. Structure development en route to perpendicular alignment as revealed by SAXS at intermediate states for the $\omega < \omega_c$ trajectory. (**A** through **C**) Two-dimensional (2D) SAXS patterns at intermediate states A, B, and C, respectively, on the top curve in Fig. 2 [see the color scales on the right; note that the number of counts at full scale increases from (A) to (C)]. The schematic diagrams at the top of each column show the orientation of the x-ray beam with respect to the sample geometry. (**D**) To compare the 2D patterns as a function of time, the three azimuthal scans for each projection are combined (A = red, B = green, and C = blue). The intensity of the azimuthal plot in the (∇**v**, **v**) plane uses an expanded scale (scale on the left, indicated by the left arrow) because the signal is so much weaker than that in the other two projections (scales on the right, indicated by the right arrows).

allel state (28).

The transverse projection remained weak throughout the fast and slow processes along both the perpendicular alignment trajectory and the parallel alignment process at frequencies near ω_c, in accord with theoretical expectations (*11*).

The pathway to the same final parallel state at very high frequencies ($10\omega_c < \omega$) differed from the one at moderately high frequencies. The early stages again converted poorly organized material into lamellae (*35*) but created transverse layers and parallel layers (Fig. 5A). This process was manifested by the distinct four-spot pattern observed when the beam was along the vorticity direction (Fig. 5A) (*37*). This bimodal character continued until the end of the fast process (Fig. 5B). At the transition from the fast to the slow process, almost all of the material was organized into layers, and in layered regions with nearly parallel orientation, the layers were tipped up and down about the $\nabla\times\mathbf{v}$ axis in domains separated by tilt-wall type boundaries (*35*). The first part of the slow process (from B to C) produced a coarsening of the spacing of the tilt walls (*35*), with an associated sharpening of the alignment into the parallel orientation (Fig. 5C). These results suggest that the motion of tilt-wall boundaries controls the slow process.

The evolution of the four-spot pattern with time is similar to that observed previously for a nearly symmetrical diblock that was ~50% longer than the present one (*26*), but in the same frequency regime ($\omega \gg \omega_c$). The higher molecular weight polymer differed from the present one in three main respects: (i) It was distinctly entangled; (ii) it was strongly segregated; and (iii) it had such a high T_{ODT} that it could not be disordered to erase its thermal and flow history but instead was subjected to a prolonged annealing to produce a reproducible initial condition. None of these three differences changed the character of the alignment trajectory in this very high–frequency regime. This result suggests that the explanation for this behavior should be general to a fairly wide range of materials, thermodynamic conditions, and shearing frequencies.

Mechanisms of Shear-Induced Alignment

The key feature that leads to the bimodal texture is that the shear frequency is so high that chain conformation cannot relax, and larger-scale structures that require the motion of many chains certainly cannot relax. Under these conditions, symmetry arguments may give insight into the physics of the alignment process. The orientations that are affected in the same way by forward and reverse cycles, and consequently have the possibility of being progressively reinforced, have fore-aft symmetry (Fig. 6A). Because the structure has insufficient time to relax, the motion imposed by the deformation in the ($\nabla\mathbf{v}$, $\mathbf{v}$) plane should dominate over out-of-plane rearrangements. These considerations leave two orientations that could potentially be reinforced by multiple cycles of high-frequency shearing: transverse and parallel (Fig. 1). Of course, this does not imply that both projections will be reinforced, but this simple symmetry argument can explain why intermediate orientations between these two, as well as orientations with normals out of the ($\nabla\mathbf{v}$, $\mathbf{v}$) plane, are not created.

The observation that a substantial transverse population forms, even though this orientation is the most unstable when subjected to shear, suggests that the mechanism for converting poorly organized domains into well-defined lamellae contrib-

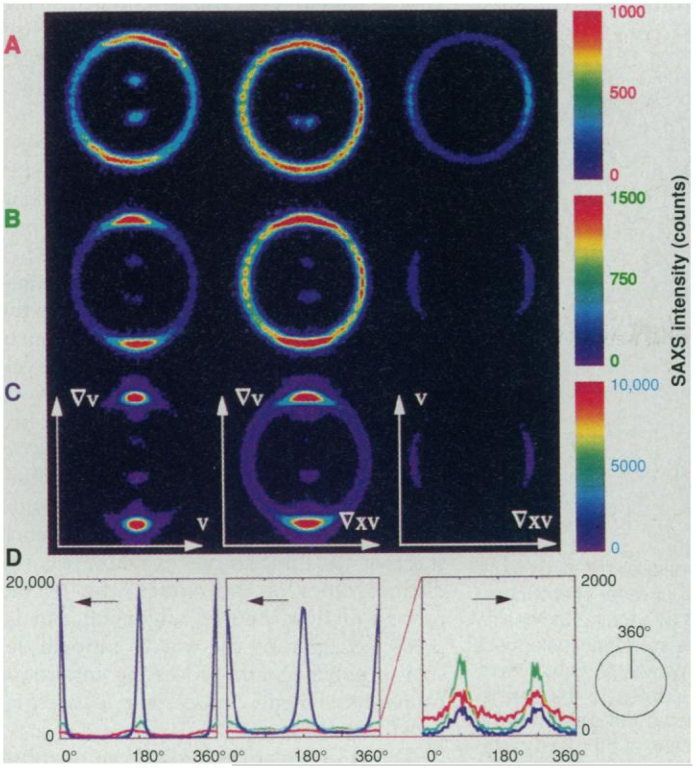

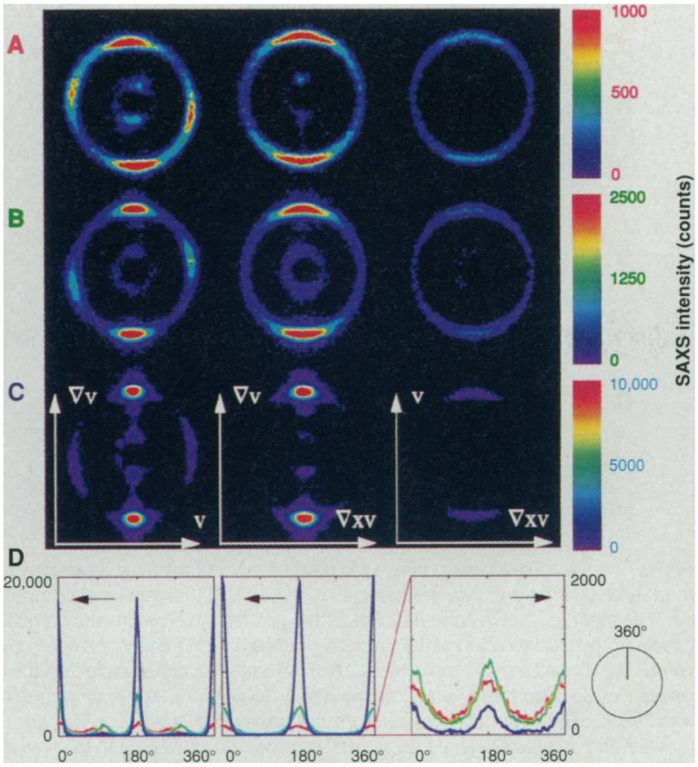

Fig. 4 (left). Structure development en route to parallel alignment for the $\omega_c < \omega < 10\omega_c$ trajectory. (**A** through **C**) 2D SAXS and (**D**) azimuthal plots for samples at intermediate states A, B, and C, indicated on the middle curve in Fig. 2. **Fig. 5 (right).** Structure development en route to parallel alignment for the $\omega \gg \omega_c$ trajectory. (**A** through **C**) 2D SAXS and (**D**) azimuthal plots for samples at intermediate states A, B, and C, indicated on the bottom curve in Fig. 2. The azimuthal plots for the ($\mathbf{v}$, $\nabla\times\mathbf{v}$) plane use an expanded scale (scale on the right, indicated by the right arrow) because the signals are much weaker than those in the other two projections (scales on the left, indicated by the left arrows).

utes approximately equally to the two possible orientations that could be reinforced [note nearly equal peak heights at point A in the azimuthal scan in the (∇v, v) plane, Fig. 5, bottom]. Simultaneous with this organization process, which creates both transverse and parallel domains, is a mechanism that converts the unstable transverse domains to the more stable parallel orientation. The former mechanism dominates at the beginning, because the initial state is largely composed of poorly organized domains; the latter dominates at long times, when most of the material exists in well-organized lamellae in either nearly transverse or nearly parallel orientation.

Here we suggest one possible mechanism for the creation of parallel and transverse lamellae that emphasizes the special feature of high frequencies $\omega \gg \omega_c$: the distortion of chain conformation. In particular, the effects of shear on the lamellar orientation and on chain conformation tend to disturb the relative orientation of the chains with respect to the layers (Fig. 6). Layers that are either transverse or parallel are disturbed equally by forward and reverse shearing, so that their orientation tends to remain unchanged. Layers that deviate from these orientations are swept into them because of the asymmetric effects of forward and reverse half-cycles of shear. For lamellae whose normal lies in the (∇v, v) plane and within ±45° of the flow direction, the half-cycle that would tend to rotate the layers away from transverse alignment also extends chains away from the layer normal, tending to resist rotation (Fig. 6B). Instead of responding in the same way to forward and reverse cycles, layers with orientation in this range would tend to rotate toward transverse alignment (Fig. 6C). For lamellae whose normal lies in the (∇v, v) plane but within ±45° of the gradient direction, the half-cycle that tends to rotate layers toward parallel alignment imposes a distortion of chain orientation from the layer normal that reinforces reorientation. This effect produces an asymmetry with respect to forward and reverse cycles that would progressively reinforce parallel alignment (Fig. 6D). Given the isotropic initial structure, equal populations of each family of local initial orientations would exist. Thus, shearing could lead to approximately equal production of transverse and parallel lamellae from the initial poorly organized material.

The trajectories to parallel alignment at moderately high frequencies ($\omega_c < \omega < 10\omega_c$) involve a transition in response: Here the initial fast process is less selective (enhancing a range of orientations, rather than just two) and has different symmetry [selecting layers with normals that lie in the (∇v, ∇×v) plane rather than the (∇v, v) plane]. This is a natural consequence of moving to frequencies that are low enough to allow relaxations on the scale of the whole chain or even the nanostructure (the time scale of the deformation approaches the single-chain relaxation time). These relaxations can produce out-of-plane reorganizations of structure that avoid higher energy distortions in the plane (such as the creation of transverse layers). In particular, all of the orientations that are enhanced during the fast process of this trajectory have the property that their layer spacing is not altered by a shearing deformation. From this distribution, the slow process winnows out all but the parallel alignment. This would be in accord with a final selection of parallel orientation at all frequencies $\omega > \omega_c$, based on the viscoelastic contrast between the styrene-rich and isoprene-rich layers (*24*).

As the frequency is lowered further, the progression of behavior continues: The fast process of the perpendicular alignment trajectory again has the type of selectivity observed in the intermediate trajectory to parallel alignment. What changes is the selectivity of the slow process. In the frequency regime where the nanostructure dominates ($\omega < \omega_c$), the selection of perpendicular alignment can be explained by the coupling of shear to composition fluctuations, which destabilizes the parallel orientation relative to the perpendicular orientation (*6*, *11*).

Thus, the progressive changes in both the fast and slow processes as one moves from very high frequencies ($\omega \gg \omega_c$) through intermediate frequencies (above, but near ω_c) to moderately low frequencies ($\omega < \omega_c$) can be qualitatively understood in terms of the changes in the relaxation processes that can occur on the time scale of the deformation. A clearer view of the nature of the fast and slow processes points the way to future modeling and simulation of dynamic processes during shear. The development of alignment from a randomly oriented initial state could be modeled in two stages: the initial conversion of poorly organized material into layers and the subsequent elimination of unfavorable orientations and defects. Once models of each stage of the process are available for the distinct types of trajectories, the overall process of flow-induced alignment can be predicted, opening the way to rational design of polymers and processing conditions to produce highly anisotropic nanostructured materials.

Direct observations provide an opportunity to reevaluate the numerous proposed mechanisms of flow alignment. The TEM and SAXS results show no evidence of selective melting or flow-induced disordering (*16*, *29*); instead, they suggest selective cre-

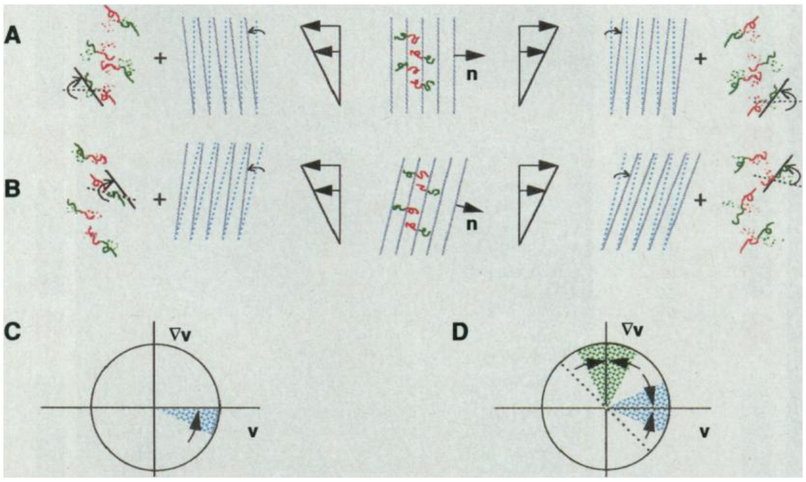

Fig. 6. The role of chain distortion in the development of the bimodal transverse-parallel texture en route to parallel alignment at high frequencies ($\omega \gg \omega_c$). The extensional component of shear affects chain conformation as shown schematically by the solid chains (deformed) compared with the dotted chains (undeformed). Convection of the layers produces a reorientation indicated by the solid lines (deformed) versus the dotted lines (undeformed). (**A**) Transverse layers are affected the same way by forward and reverse cycles, so there is no net tendency to reorient. A similar argument applies to the parallel orientation. (**B**) Layers tilted away from the transverse orientation are not affected the same way by forward and reverse shear. If their normal **n** is tilted down relative to the flow direction of a forward cycle, then the distortion of the chains is stronger in the forward than in the reverse direction; consequently, the net effect of a full cycle is to promote reorientation toward transverse alignment. (**C**) Thus, layers with **n** in the blue-shaded sector will tend to evolve toward transverse alignment (**n** ∥ **v**). (**D**) The same reasoning applies to orientations tilted in the opposite direction relative to transverse alignment, so they will also tend to evolve toward transverse alignment (blue-shaded region). Similarly, orientations tilted away from parallel alignment would progressively rotate into parallel alignment (green-shaded regions).

ation of well-defined nanostructure from poorly organized regions, particularly in the initial fast processes of various alignment trajectories. The concept of defect migration (*3*) is made specific, in terms of both the type of defects involved and the dynamic regime where they are important (for example, coarsening of chevron patterns in the slow process of parallel alignment in the very high–frequency regime). Bimodal textures that have been observed in disparate systems (*20–22, 26*) can be viewed in a unified way and explained by the role of conformational distortion of the polymer chains, without invoking entanglement or strong segregation (*26*). This powerful experimental approach is being extended to other nanostructures, including the elaborate structures formed by ABC triblock copolymers. Progress in other systems will open the way to insights, such as those for lamellar diblocks, that will guide novel processing strategies for a wide range of self-assembled nanostructures.

REFERENCES AND NOTES

1. F. S. Bates, *Science* **251**, 898 (1991); ——— and G. H. Fredrickson, *Annu. Rev. Phys. Chem.* **41**, 525 (1990); *Annu. Rev. Mater. Sci.* **26**, 501 (1996); R. H. Colby, *Curr. Opin. Colloid Interface Sci.* **1**, 454 (1996).
2. A. Keller, E. Pedemonte, E. M. Willmouth, *Colloid Polym. Sci.* **238**, 25 (1970); M. J. Folkes, A. Keller, F. P. Scalisi, *ibid.* **251**, 1 (1973).
3. G. Hadziioannou, A. Mathis, A. Skoulious, *ibid.* **257**, 136 (1979).
4. F. A. Morrison and H. H. Winter, *Macromolecules* **22**, 3533 (1989); ———, W. Gronski, J. D. Barnes, *ibid.* **23**, 4200 (1990).
5. M. E. Cates and S. T. Milner, *Phys. Rev. Lett.* **62**, 1856 (1989); Z.-G. Wang, *J. Chem. Phys.* **100**, 2298 (1994); S. Qi and Z.-G. Wang, *Phys. Rev. E* **55**, 1682 (1997).
6. M. Goualian and S. T. Milner, *Phys. Rev. Lett.* **74**, 1775 (1995); G. H. Fredrickson, *J. Rheol.* **38**, 1045 (1994).
7. J. T. Chen, E. L. Thomas, C. K. Ober, G.-p. Mao, *Science* **273**, 343 (1996); S. I. Stupp *et al.*, *ibid.* **276**, 384 (1997); S. Kanaoka and R. H. Grubbs, *Macromolecules* **28**, 4707 (1995); X. L. Chen and S. A. Jenekhe, *ibid.* **29**, 6189 (1996); M. Park, C. Harrison, P. M. Chaikin, R. A. Register, D. H. Adamson, *Science* **276**, 1401 (1997).
8. W. M. Gelbart and A. Benshaul, *J. Phys. Chem.* **100**, 13169 (1996); J. Liu *et al.*, *Adv. Colloid Interface Sci.* **69**, 131 (1996); P. Pieranski, *Contemp. Phys.* **24**, 25 (1983); J. M. Jethmalani and W. T. Ford, *Chem. Mater.* **8**, 2138 (1996).
9. W. Richtering, G. Schmidt, P. Lindner, *Colloid Polym. Sci.* **274**, 85 (1996); U. Olsson and K. Mortensen, *J. Phys. II* **5**, 789 (1995); O. Diat, D. C. Roux, F. Nallet, *ibid.* **3**, 1427 (1993); L. Soubiran, C. Coulon, P. Sierro, D. Roux, *Europhys. Lett.* **31**, 243 (1995); C. R. Safinya *et al.*, *Science* **261**, 588 (1993).
10. N. K. Raman, M. T. Anderson, C. J. Brinker, *Chem. Mater.* **8**, 1682 (1996); Q. Huo, R. Leon, P. M. Petroff, G. D. Stucky, *Science* **268**, 1324 (1995); E. Evans, H. Bowman, A. Leung, D. Needham, D. Tirrell, *Science* **273**, 933 (1996); K. M. McGrath and C. J. Drummond, *Colloid Polym. Sci.* **274**, 612 (1996).
11. R. Bruinsma and Y. Rabin, *Phys. Rev. A* **45**, 994 (1992).
12. W. D. Dozier and P. M. Chaikin, *J. Physique* **43**, 843 (1982); J. Liu, D. A. Weitz, B. J. Ackerson, *Phys. Rev. E* **48**, 1106 (1993).
13. M. R. Ghadiri, *Adv. Mater.* **7**, 675 (1995); W. Frey *et al.*, *Proc. Natl. Acad. Sci. U.S.A.* **93**, 4937 (1996).
14. U. Krappe, R. Stadler, I. Voigt-Martin, *Macromolecules* **28**, 4558 (1995); J. Bechmann, C. Auschra, R. Stadler, *Macromol. Rapid Commun.* **15**, 67 (1994); Z. Wei and Z.-G. Wang, *Macromolecules* **28**, 7215 (1995).
15. K. Amundson *et al.*, *Macromolecules* **24**, 6546 (1991); K. Amundson, E. Helfand, X. Quan, S. D. Smith, *ibid.* **26**, 2698 (1993); K. Amundson, E. Helfand, X. N. Quan, S. D. Hudson, S. D. Smith, *ibid.* **27**, 6559 (1994); T. L. Morkved *et al.*, *Science* **273**, 931 (1996).
16. K. Koppi, M. Tirrell, F. S. Bates, K. Almdal, R. H. Colby, *J. Phys. II* **2**, 1941 (1992).
17. R. J. Albalak and E. L. Thomas, *J. Polym. Sci. Polym. Phys. Ed.* **31**, 37 (1993).
18. H. H. Lee, R. A. Register, D. A. Hajduk, S. M. Gruner, *Polym. Eng. Sci.* **36**, 1414 (1996).
19. R. G. Larson, K. I. Winey, S. S. Patel, H. Watanabe, *Rheol. Acta* **32**, 245 (1993); K. I. Winey, S. S. Patel, R. G. Larson, H. Watanabe, *Macromolecules* **26**, 2542 (1993); *ibid.*, p. 4373; B. L. Riise, G. H. Fredrickson, R. G. Larson, D. S. Pearson, *ibid.* **28**, 7653 (1995).
20. S. D. Hudson, K. R. Amundson, H. G. Jeon, S. D. Smith, *Mater. Res. Soc. Bull.* **20**, 42 (1995).
21. B. S. Pinheiro, D. A. Hajduk, S. M. Gruner, K. I. Winey, *Macromolecules* **29**, 1482 (1996).
22. S. Okamoto, K. Saijo, T. Hashimoto, *ibid.* **27**, 5547 (1994).
23. R. M. Kannan and J. A. Kornfield, *ibid.*, p. 1177.
24. S. S. Patel, R. G. Larson, K. I. Winey, H. Watanabe, *ibid.* **28**, 4313 (1995).
25. Y. Zhang, U. Wiesner, H. W. Spiess, *ibid.*, p. 778.
26. Y. Zhang and U. Wiesner, *J. Chem. Phys.* **103**, 4784 (1995).
27. V. K. Gupta, R. Krishnamoorti, J. A. Kornfield, S. D. Smith, *Macromolecules* **28**, 4464 (1995); *ibid.* **29**, 1359 (1996).
28. V. K. Gupta *et al.*, *ibid.* **29**, 875 (1996).
29. N. P. Balsara and H. J. Dai, *J. Chem. Phys.* **105**, 2942 (1996); K. Koppi, M. Tirrell, F. S. Bates, *Phys. Rev. Lett.* **70**, 1449 (1993); H. Wang, P. K. Kesani, N. P. Balsara, B. Hammouda, *Macromolecules* **30**, 982 (1997).
30. D. Maring and U. Wiesner, *Macromolecules* **30**, 660 (1997).
31. Y. Zhang, U. Wiesner, Y. Yang, T. Pakula, H. W. Spiess, *ibid.* **29**, 5427 (1996).
32. In addition to frequency, the strain amplitude, temperature, and thermal history can all modify the selection of alignment in certain regimes (*27, 30, 31*). The rate and even the direction of alignment are influenced by the amplitude of the oscillatory shear (*27, 30*); temperature enters primarily through its effect on the relaxation dynamics of the chains (*24, 28*), and annealing can alter alignment behavior at very low frequencies (*33, 31*).
33. This low-frequency regime ($\omega < \omega_d$) seems to be controlled by frequency in poly(ethylene-*alt*-propylene)-*block*-(ethylethylene) (PEP-PEE) (*16, 23*). However, it is sensitive to thermal history in poly(styrene-*block*-isoprene) (PS-PI): The perpendicular alignment regime extends to the lowest accessible frequencies in PS-PI unless the sample is subjected to prolonged annealing at temperatures close to the upper glass transition of the system (>8 hours at $T_{g,\mathrm{PS\text{-}rich}}$ + 20°C) (*31*).
34. H. Kodamaand and M. Doi, *Macromolecules* **29**, 2652 (1996).
35. Z.-R. Chen *et al.*, *ibid.*, in press.
36. There is one family of trajectories that remains to be investigated in the future: the route to parallel alignment at very low frequencies ($\omega < \omega_d$). This regime has been studied by rheo-optical techniques in PEP-PEE-2, but this system is not amenable to TEM. In PS-PI, this regime is not accessible without a prolonged annealing treatment (*33*), which is beyond the scope of the present study.
37. Bimodal transverse-parallel distributions (four-spot SAXS patterns) have been observed in lamellar diblocks with strong viscoelastic contrast in the high-frequency regime ($\omega \gg \omega_c$) (*21, 22, 26*), and their probable correspondence to trajectories with negative Δn_{13} has been noted (*28*).

38. This research was carried out with the support of NSF (grant CTS 9421015), the Air Force Office of Scientific Research (Liquid Crystals MURI), Chevron, and Raychem.